Electronic Supplementary Information

Rapid Parallel Generation of a Fluorescently Barcoded Drop Library from a Microtiter Plate Using the Plate-Interfacing Parallel Encapsulation (PIPE) Chip

Geoffrey K. Zath[1,2]‡, Ralph A. Sperling[4,5]‡, Carter W. Hoffman[1,2], Dimitri A. Bikos[1,2], Reha Abbasi[1,2], Adam R. Abate[6], David A. Weitz[4,7], Connie B. Chang[1,2,3]*

[1]Center for Biofilm Engineering, Montana State University, Bozeman, MT, USA

[2]Department of Chemical and Biological Engineering, Montana State University, Bozeman, MT, USA

[3]Department of Physiology and Biomedical Engineering, Mayo Clinic, Rochester, MN, USA

[4]Department of Physics, School of Engineering and Applied Sciences, Harvard University, Cambridge, MA, USA

[5]Fraunhofer Institute for Microengineering and Microsystems IMM, Mainz, Germany

[6]Department of Bioengineering and Therapeutic Sciences, University of California, San Francisco, CA, USA

[7]Wyss Institute for Biologically Inspired Engineering at Harvard University, Boston, MA, USA

‡ Authors contributed equally

*To whom correspondence may be addressed: Connie B. Chang, Department of Physiology and Biomedical Engineering, Mayo Clinic, 200 1st St SW, Rochester, MN 55902, conniebchang@gmail.com

Table of contents

1. PIPE Chip Fabrication

Negative master molds were fabricated upon 3-in diameter silicon wafers (University Wafer, ID# 447, test grade) using UV cross-linked SU-8 photoresist exposed through photomasks printed on high-resolution transparent plastic film (CAD Art, 20k dpi). The top (Fig. 1a, i) and middle (Fig. 1a, ii) layer negative master molds were made with SU-8 2075 (MicroChem) to create 250 μm tall channels while the bottom layer (Fig. 1a, iii) was made with SU-8 3050 (MicroChem) to create 50 μm tall channels. To create the 250 μm tall channels, a first coat of SU-8 2075 was spun at 1000 rpm for 30 s, then softbaked at 100 °C for 60 min, and resulted in a ~200 μm thick layer. The second coat of SU-8 2075 was spun at 3000 rpm for 30 s, then softbaked at 100 °C for 10 min, and resulted in a ~250 thick layer. To create the 50 μm tall channels, SU-8 3050 was spun at 3000 rpm for 30 s, then softbaked at 95 °C for 15 min. For all spin coating conditions, photoresist was initially spun at 500 rpm for 10 s to evenly coat the wafer surface. PDMS prepolymer (Sylgard 184, 10:1 mix ratio of prepolymer to curing agent) was cast onto the negative master molds and cured overnight at 65°C. The cross-linked PDMS devices were cut out using a scalpel. Via holes

and sample inlet holes were manually punched using a 0.75 mm ID biopsy punch (Harris Unicore). A larger 1.25 mm ID biopsy punch (Robbins Instruments RBP-12) was used to fit 1/16-in OD tubing (IDEX FEP tubing) to the oil inlet and 0.052-in OD tubing (Scientific Commodities PE/5) to the drop outlet port on the top layer (Fig. 1a, i) of the device. Assembly of the PIPE chip began with oxygen plasma treatment (Harrick Plasma PDC-001) of the middle (Fig. 1a, ii) and bottom (Fig. 1a, iii) PDMS layers for 30 s at medium power and 700 mTorr oxygen pressure. A thin layer of deionized (DI) water was introduced between the plasma-treated surfaces to temporarily prevent the PDMS layers from bonding during the alignment process, which was accomplished by eye. The aligned layers were immediately baked for ≥1 h in a 65 °C oven to dry the DI water and allow the PDMS layers to bond. The top face of the bonded two-layer device was subjected to oxygen plasma (Fig. 1a, i) of the device with the previously mentioned plasma treatment settings. DI water was introduced to prevent bonding while the top layer (Fig. 1a, i) was aligned with the previously bonded middle (Fig. 1a, ii) and bottom (Fig. 1a, iii) layers such that the via holes of the middle layer (Fig. 1a, ii) connect with their respective oil inlet and drop outlet channels. Device channels were made hydrophobic by flowing Aquapel (Pittsburgh Glass Works) through the channels of the bonded device, flushing with compressed air, and baking in a 65 °C drying oven for ≥1 h to complete the reaction.

2. Microbead and Quantum Dot Barcode Label Combinations

Table S1 Green and red microbead barcode concentration combinations.

#	Green microbeads (beads/μL)	Red microbeads (beads/μL)	#	Green microbeads (beads/μL)	Red microbeads (beads/μL)
1	5.1×10^5	5.1×10^5	13	2.3×10^6	2.3×10^6
2	1.3×10^6	5.1×10^5	14	3.6×10^6	2.3×10^6
3	2.3×10^6	5.1×10^5	15	5.1×10^6	2.3×10^6
4	3.6×10^6	5.1×10^5	16	5.1×10^5	3.6×10^6
5	5.1×10^6	5.1×10^5	17	1.3×10^6	3.6×10^6
6	5.1×10^5	1.3×10^6	18	2.3×10^6	3.6×10^6
7	1.3×10^6	1.3×10^6	19	3.6×10^6	3.6×10^6
8	2.3×10^6	1.3×10^6	20	5.1×10^6	3.6×10^6
9	3.6×10^6	1.3×10^6	21	5.1×10^5	5.1×10^6
10	5.1×10^6	1.3×10^6	22	1.3×10^6	5.1×10^6
11	5.1×10^5	2.3×10^6	23	2.3×10^6	5.1×10^6
12	1.3×10^6	2.3×10^6	24	3.6×10^6	5.1×10^6

Table S2 QD625 and QD705 quantum dot barcode concentration combinations.

#	QD625 (pM)	QD705 (pM)	#	QD625 (pM)	QD705 (pM)	#	QD625 (pM)	QD705 (pM)	#	QD625 (pM)	QD705 (pM)
1	1.15×10^4	1.02×10^4	49	1.15×10^4	5.76×10^3	97	1.15×10^4	2.56×10^3	145	1.15×10^4	6.40×10^2
2	9.68×10^3	1.02×10^4	50	9.68×10^3	5.76×10^3	98	9.68×10^3	2.56×10^3	146	9.68×10^3	6.40×10^2
3	8.00×10^3	1.02×10^4	51	8.00×10^3	5.76×10^3	99	8.00×10^3	2.56×10^3	147	8.00×10^3	6.40×10^2
4	6.48×10^3	1.02×10^4	52	6.48×10^3	5.76×10^3	100	6.48×10^3	2.56×10^3	148	6.48×10^3	6.40×10^2
5	5.12×10^3	1.02×10^4	53	5.12×10^3	5.76×10^3	101	5.12×10^3	2.56×10^3	149	5.12×10^3	6.40×10^2
6	3.92×10^3	1.02×10^4	54	3.92×10^3	5.76×10^3	102	3.92×10^3	2.56×10^3	150	3.92×10^3	6.40×10^2
7	2.88×10^3	1.02×10^4	55	2.88×10^3	5.76×10^3	103	2.88×10^3	2.56×10^3	151	2.88×10^3	6.40×10^2
8	2.00×10^3	1.02×10^4	56	2.00×10^3	5.76×10^3	104	2.00×10^3	2.56×10^3	152	2.00×10^3	6.40×10^2
9	1.28×10^3	1.02×10^4	57	1.28×10^3	5.76×10^3	105	1.28×10^3	2.56×10^3	153	1.28×10^3	6.40×10^2
10	7.20×10^2	1.02×10^4	58	7.20×10^2	5.76×10^3	106	7.20×10^2	2.56×10^3	154	7.20×10^2	6.40×10^2
11	3.20×10^2	1.02×10^4	59	3.20×10^2	5.76×10^3	107	3.20×10^2	2.56×10^3	155	3.20×10^2	6.40×10^2
12	8.00×10^1	1.02×10^4	60	8.00×10^1	5.76×10^3	108	8.00×10^1	2.56×10^3	156	8.00×10^1	6.40×10^2
13	1.15×10^4	9.00×10^3	61	1.15×10^4	4.84×10^3	109	1.15×10^4	1.96×10^3	157	1.15×10^4	3.60×10^2
14	9.68×10^3	9.00×10^3	62	9.68×10^3	4.84×10^3	110	9.68×10^3	1.96×10^3	158	9.68×10^3	3.60×10^2
15	8.00×10^3	9.00×10^3	63	8.00×10^3	4.84×10^3	111	8.00×10^3	1.96×10^3	159	8.00×10^3	3.60×10^2
16	6.48×10^3	9.00×10^3	64	6.48×10^3	4.84×10^3	112	6.48×10^3	1.96×10^3	160	6.48×10^3	3.60×10^2
17	5.12×10^3	9.00×10^3	65	5.12×10^3	4.84×10^3	113	5.12×10^3	1.96×10^3	161	5.12×10^3	3.60×10^2
18	3.92×10^3	9.00×10^3	66	3.92×10^3	4.84×10^3	114	3.92×10^3	1.96×10^3	162	3.92×10^3	3.60×10^2
19	2.88×10^3	9.00×10^3	67	2.88×10^3	4.84×10^3	115	2.88×10^3	1.96×10^3	163	2.88×10^3	3.60×10^2
20	2.00×10^3	9.00×10^3	68	2.00×10^3	4.84×10^3	116	2.00×10^3	1.96×10^3	164	2.00×10^3	3.60×10^2
21	1.28×10^3	9.00×10^3	69	1.28×10^3	4.84×10^3	117	1.28×10^3	1.96×10^3	165	1.28×10^3	3.60×10^2
22	7.20×10^2	9.00×10^3	70	7.20×10^2	4.84×10^3	118	7.20×10^2	1.96×10^3	166	7.20×10^2	3.60×10^2
23	3.20×10^2	9.00×10^3	71	3.20×10^2	4.84×10^3	119	3.20×10^2	1.96×10^3	167	3.20×10^2	3.60×10^2
24	8.00×10^1	9.00×10^3	72	8.00×10^1	4.84×10^3	120	8.00×10^1	1.96×10^3	168	8.00×10^1	3.60×10^2
25	1.15×10^4	7.84×10^3	73	1.15×10^4	4.00×10^3	121	1.15×10^4	1.44×10^3	169	1.15×10^4	1.60×10^2
26	9.68×10^3	7.84×10^3	74	9.68×10^3	4.00×10^3	122	9.68×10^3	1.44×10^3	170	9.68×10^3	1.60×10^2
27	8.00×10^3	7.84×10^3	75	8.00×10^3	4.00×10^3	123	8.00×10^3	1.44×10^3	171	8.00×10^3	1.60×10^2
28	6.48×10^3	7.84×10^3	76	6.48×10^3	4.00×10^3	124	6.48×10^3	1.44×10^3	172	6.48×10^3	1.60×10^2
29	5.12×10^3	7.84×10^3	77	5.12×10^3	4.00×10^3	125	5.12×10^3	1.44×10^3	173	5.12×10^3	1.60×10^2
30	3.92×10^3	7.84×10^3	78	3.92×10^3	4.00×10^3	126	3.92×10^3	1.44×10^3	174	3.92×10^3	1.60×10^2
31	2.88×10^3	7.84×10^3	79	2.88×10^3	4.00×10^3	127	2.88×10^3	1.44×10^3	175	2.88×10^3	1.60×10^2
32	2.00×10^3	7.84×10^3	80	2.00×10^3	4.00×10^3	128	2.00×10^3	1.44×10^3	176	2.00×10^3	1.60×10^2
33	1.28×10^3	7.84×10^3	81	1.28×10^3	4.00×10^3	129	1.28×10^3	1.44×10^3	177	1.28×10^3	1.60×10^2
34	7.20×10^2	7.84×10^3	82	7.20×10^2	4.00×10^3	130	7.20×10^2	1.44×10^3	178	7.20×10^2	1.60×10^2
35	3.20×10^2	7.84×10^3	83	3.20×10^2	4.00×10^3	131	3.20×10^2	1.44×10^3	179	3.20×10^2	1.60×10^2
36	8.00×10^1	7.84×10^3	84	8.00×10^1	4.00×10^3	132	8.00×10^1	1.44×10^3	180	8.00×10^1	1.60×10^2
37	1.15×10^4	6.76×10^3	85	1.15×10^4	3.24×10^3	133	1.15×10^4	1.00×10^3	181	1.15×10^4	4.00×10^1
38	9.68×10^3	6.76×10^3	86	9.68×10^3	3.24×10^3	134	9.68×10^3	1.00×10^3	182	9.68×10^3	4.00×10^1
39	8.00×10^3	6.76×10^3	87	8.00×10^3	3.24×10^3	135	8.00×10^3	1.00×10^3	183	8.00×10^3	4.00×10^1
40	6.48×10^3	6.76×10^3	88	6.48×10^3	3.24×10^3	136	6.48×10^3	1.00×10^3	184	6.48×10^3	4.00×10^1
41	5.12×10^3	6.76×10^3	89	5.12×10^3	3.24×10^3	137	5.12×10^3	1.00×10^3	185	5.12×10^3	4.00×10^1
42	3.92×10^3	6.76×10^3	90	3.92×10^3	3.24×10^3	138	3.92×10^3	1.00×10^3	186	3.92×10^3	4.00×10^1
43	2.88×10^3	6.76×10^3	91	2.88×10^3	3.24×10^3	139	2.88×10^3	1.00×10^3	187	2.88×10^3	4.00×10^1
44	2.00×10^3	6.76×10^3	92	2.00×10^3	3.24×10^3	140	2.00×10^3	1.00×10^3	188	2.00×10^3	4.00×10^1
45	1.28×10^3	6.76×10^3	93	1.28×10^3	3.24×10^3	141	1.28×10^3	1.00×10^3	189	1.28×10^3	4.00×10^1
46	7.20×10^2	6.76×10^3	94	7.20×10^2	3.24×10^3	142	7.20×10^2	1.00×10^3	190	7.20×10^2	4.00×10^1
47	3.20×10^2	6.76×10^3	95	3.20×10^2	3.24×10^3	143	3.20×10^2	1.00×10^3	191	3.20×10^2	4.00×10^1
48	8.00×10^1	6.76×10^3	96	8.00×10^1	3.24×10^3	144	8.00×10^1	1.00×10^3	192	8.00×10^1	4.00×10^1

3. PIPE Chip Drop Formation Characterization

Reynolds Number Calculation. The Reynolds number was calculated independently for the water and oil phases as $Re = \frac{\rho v d}{\mu}$ where ρ is the fluid density (0.997 g/mL for water and 1.614 g/mL for HFE 7500), v is the fluid velocity (maximum of 0.4 m/s for water and 0.9 m/s for oil), d is the hydraulic diameter ($2w_{channel}$ for a square channel, or 100 μm), and μ is the dynamic viscosity (0.881 mPa·s for water and 1.243 mPa·s for oil). A maximum Reynolds number of 45 was calculated for the water inlet channel and 58 for the oil inlet channel. For laminar flow at a low Reynolds number (Re < 60 for PIPE chip operation), a linear correlation between P and Q is expected based upon the Hagen-Poiseuille relationship ($\Delta P = \frac{8\mu l}{\pi r^4} Q$). We generated a standard curve which verifies that Q_{water}/Q_{oil} is linearly correlated with P_{water}/P_{oil} (R^2 = 0.916) (Fig. S1).

Convert L_{drop} to V_{drop}. To fit the data of V_{drop} as a function of Q_{water}/Q_{oil} in Fig 3c, we converted L_{drop} to V_{drop} in the drop with a scaling law,[1] which relates drop length (L_{drop}) to Q_{water}/Q_{oil} (Equation 1). The V_{drop} is converted by approximating a drop in a channel as having a capsule geometry where $V_{drop} = \frac{\pi}{4} w_{channel}^2 (L_{drop} - \frac{1}{3} w_{channel})$.

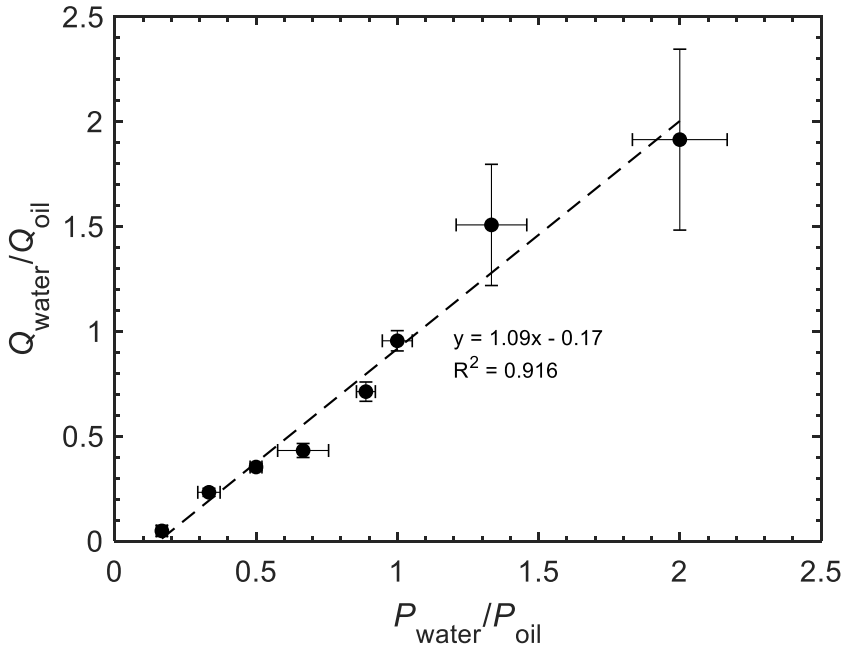

Fig. S1 Standard curve relating volumetric flowrate ratio to pressure ratio during PIPE chip operation. The relationship between the water/oil pressure ratio (P_{water}/P_{oil}) and water/oil volumetric flowrate ratio (Q_{water}/Q_{oil}) is linear. Error bars on the x-axis represent gauge error and error bars on the y-axis represent one standard deviation of volume measurements.

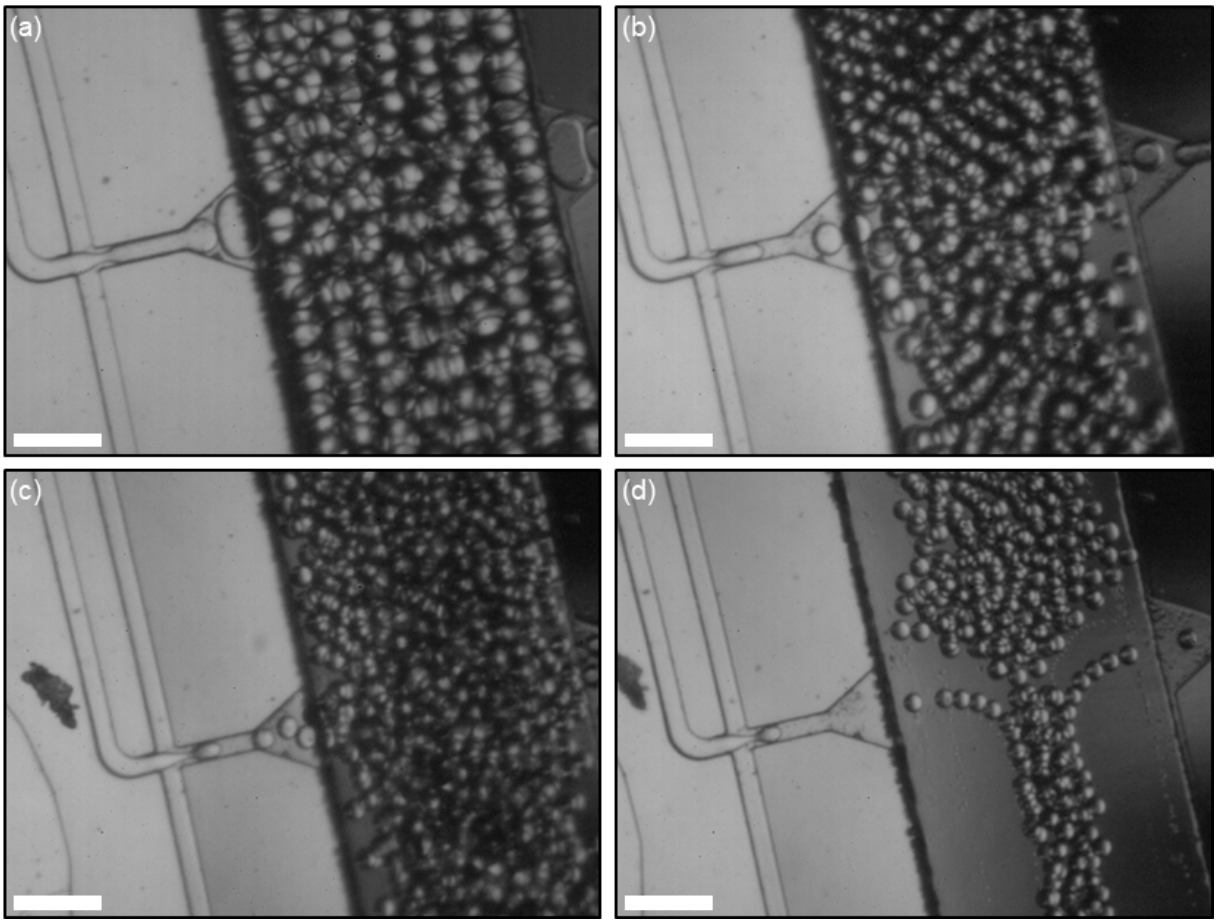

Video S1 High speed video capture of drop formation in the PIPE chip ordered by descending D_{drop}, for (a) high water pressure (■, P_{water} = 6 psig and P_{oil} = 3 psig, P_{water}/P_{oil} = 2), (b) low combined pressure (▼, P_{water} = 2 psig and P_{oil} = 3 psig, P_{water}/P_{oil} = 0.67), (c) high combined pressure (▲, P_{water} = 8 and P_{oil} = 12 psig, P_{water}/P_{oil} = 0.67), (d) and high oil pressure (♦, P_{water} = 2 psig and P_{oil} = 12 psig, P_{water}/P_{oil} = 0.17) conditions. Scale bars are 500 μm.

4. Barcoded Drop Detection

The drop fluorescence detection system for the microbead barcoded drop library consisted of a custom modified Nikon Diaphot 300 inverted microscope with two lasers, a set of dichroic mirrors and photomultiplier tubes (PMTs, Hamamatsu H10723-20).[2] The beams of the 50 mW, 473 nm laser (Suzhou Daheng Optics and Fine Mechanics Co., DHOM-W473-50mW) and the 50 mW, 405 nm laser (Changchun New Industries Optoelectronics Tech Co., MDL-III-405-50mW) were aligned together and coupled into the backport of the microscope where they were focused to a spot by the objective (40×, NA 0.60, Motic). The flowing of drops across the laser spot resulted in fluorescence detection by three PMTs split into three channels using dichroic and bandpass filters, Ch1: 445/40 nm (blue), Ch2: 525/50 nm (green), Ch3: >561 nm (red). A schematic of the drop fluorescence detection system and a detailed optical path representation are provided in Fig. S4. For bright field illumination, the light from the incandescent bulb was filtered by a 785/62 nm near-infrared (NIR) bandpass filter in order to not interfere with fluorescence detection measurements. A field programmable gate array (FPGA, National Instruments NI-7852R) was used to control the PMT gains and record fluorescence measurements using LabVIEW 2015.

The detection system for quantum dot barcoding consisted of a custom modified microscope, similar to the one described above. The beam of the laser (488 nm, 25 mW, Picarro) was coupled into the backport of the microscope and focused to a spot by the objective (40×, 0.85 NA, Leica). The light was split into three colors for fluorescent detection by using dichroic and bandpass filters for each channel, Ch1: 536/40 nm (green), Ch2: 632/22 nm (red), Ch3: 716/40 nm (far-red), and detected by a PMT for each channel.

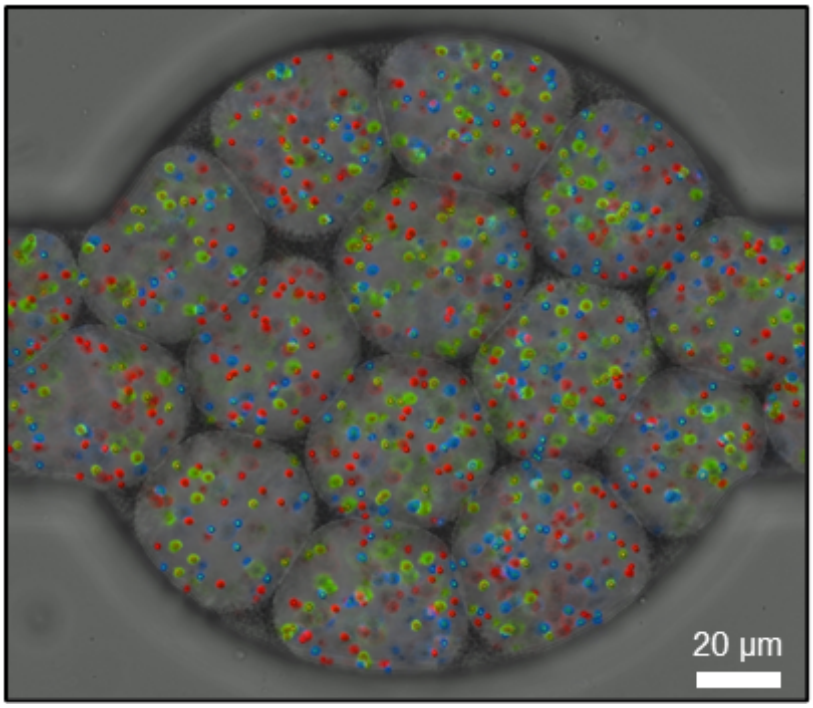

Fig. S2 Confocal image of fluorescent blue, green, and red microbeads in drops.

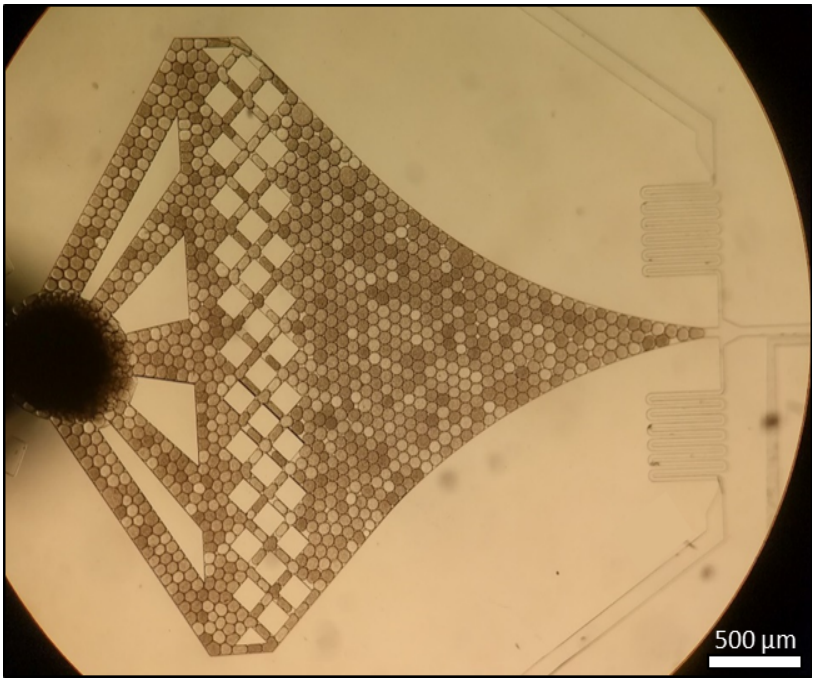

Fig. S3 Re-injection of barcoded drops into a detection chip. The shading of drops is due to the various microbead concentrations encapsulated in the drops.

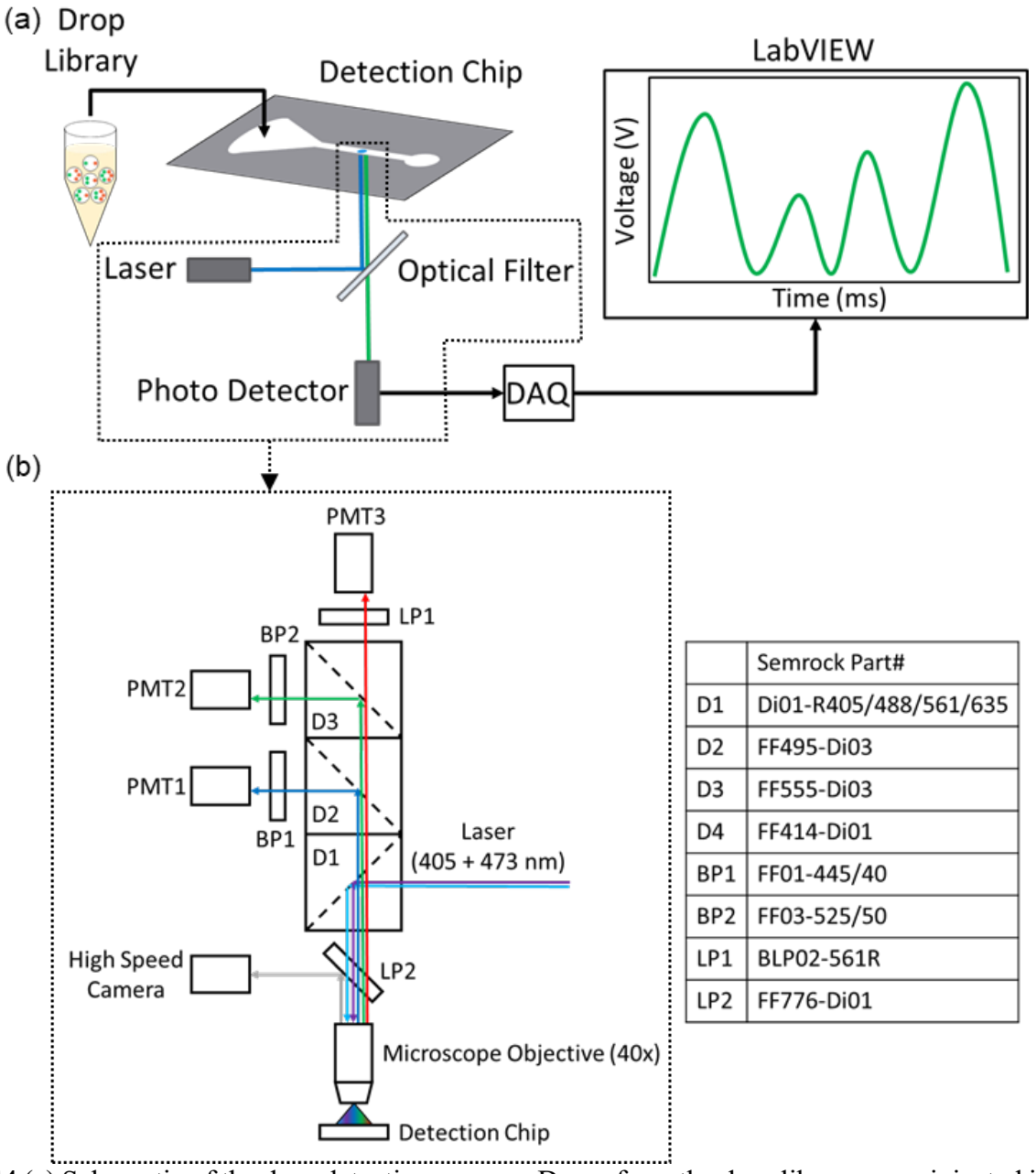

	Semrock Part#
D1	Di01-R405/488/561/635
D2	FF495-Di03
D3	FF555-Di03
D4	FF414-Di01
BP1	FF01-445/40
BP2	FF03-525/50
LP1	BLP02-561R
LP2	FF776-Di01

Fig. S4 (a) Schematic of the drop detection process. Drops from the drop library are reinjected into a detection chip mounted on the stage of a fluorescence detection microscope. The optical filter system allows laser light to be reflected towards the fluorescent barcoded drop while allowing emitted light from the drop to be detected by a photodetector in-line with the drop. The output of the photo detector is collected by a data acquisition device (DAQ) and then processed and recorded in a custom LabVIEW program. (b) Optical path for fluorescent drop detection. Coupled laser light enters the PMT stack and is reflected to the objective by the first dichroic mirror (D1). Emitted fluorescence passes through the first dichroic mirror (D1) and blue light is reflected by the second dichroic (D2), filtered by the first bandpass filter (BP1), and detected by the channel 1 PMT (PMT1). This process is repeated for green light while all red light above a wavelength of 555 nm is collected by PMT3. A 776 nm longpass filter (LP2) allows for transmitted light to be captured by a high-speed camera during fluorescent drop detection.

5. Discrimination of Discrete Signals in Barcoded Drop Libraries

Drop Library Clustering. The clustering algorithm Density-Based Spatial Clustering of Applications with Noise (DBSCAN)[3] was used to assign each drop detected to a cluster related to a specific barcode in the microbead and quantum dot barcoded drop library. DBSCAN is a density-based clustering method that groups together closely packed data points and marks outliers which lie in low-density regions as noise. Drops containing the same concentration of a fluorescence barcode should emit the same fluorescence signal, while factoring in signal noise, and will therefore create a data cluster that DBSCAN can find and tag with a specific identification code. DBSCAN uses two parameters for clustering, *minPts* defines the minimum number of data to include in a cluster and ε represents the maximum allowable distance between data in a cluster. The DBSCAN function in MATLAB was used for clustering data (introduced in MATLAB R2019a). For microbead barcoding, *minPts* was set to 50 and ε was set to 2.8×10^{-2} while for quantum dot barcoding, *minPts* was set to 25 and ε was set to 1×10^{-4}.

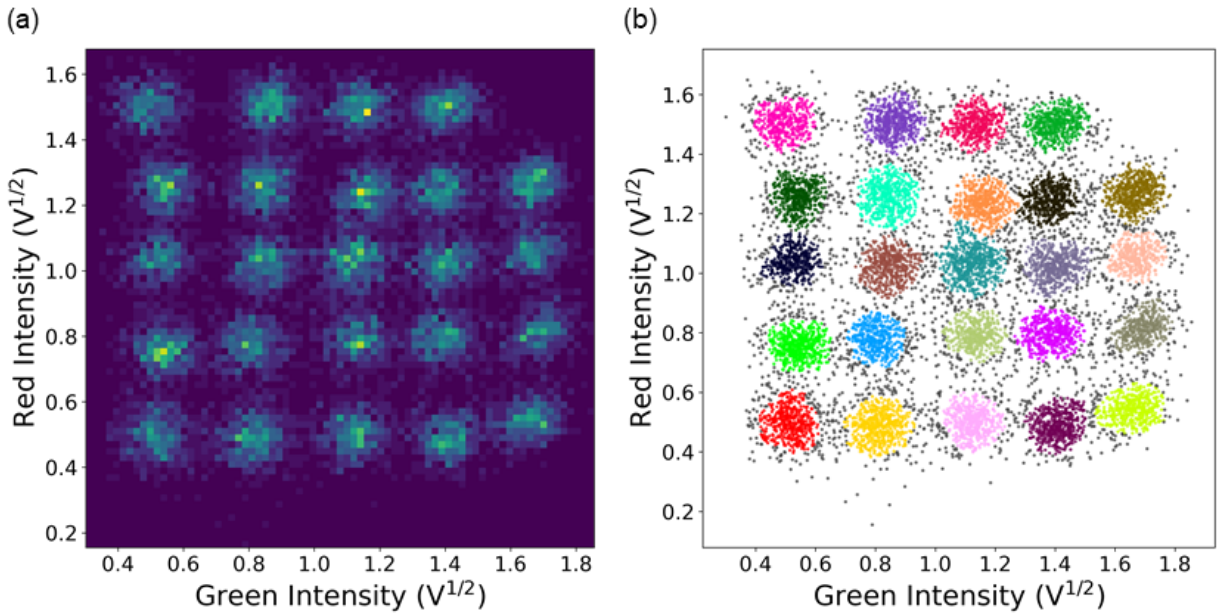

Fig. S5: Additional plots of the microbead drop library data using a (a) heatmap and (b) DBSCAN clustering where each cluster is labeled a different color and noise is shown in gray. The data was corrected for the spectral overlap here to better show the grid of barcoded clusters. To correct for the overlap, the compensation matrix [[1, -0.42], [-0.05, 1]] was applied.

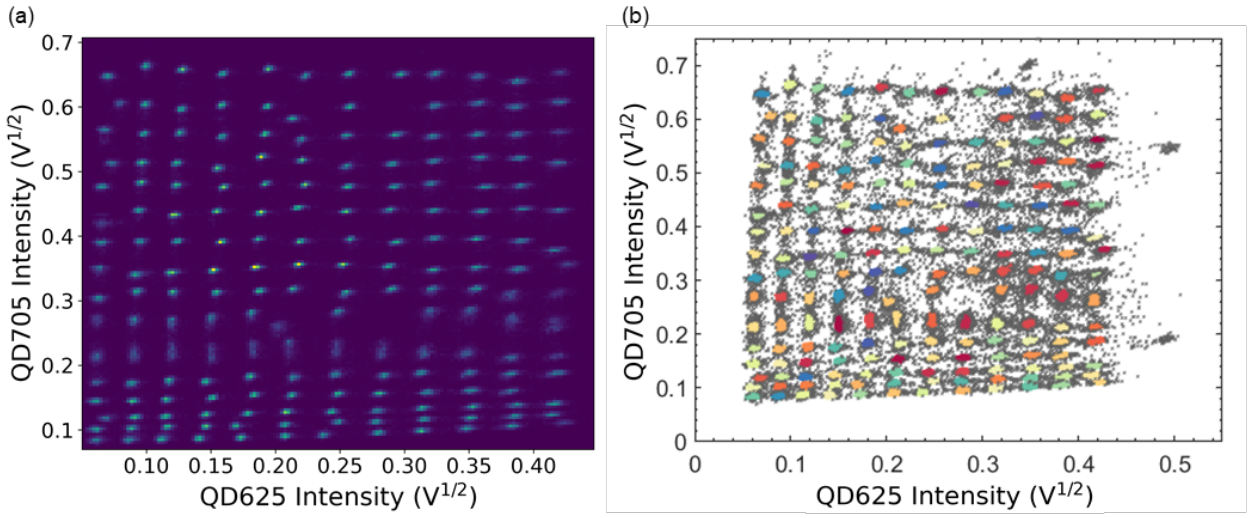

Fig. S6: Additional plots of the quantum dot drop library data using a (a) heatmap and (b) DBSCAN clustering where each cluster is labeled a different color and noise is shown in gray. Here, spectral overlap has not been corrected.

Schottky Equation. The Schottky equation adapted for PMTs with a voltage output,[4, 5] approximates shot noise and is defined here as:

$$\sigma_{\text{shot}} = \sqrt{\mu_{\text{itensity}} C G e \pi f_{\text{3dB}}} \qquad \text{(Eq. S1)}$$

where σ_{shot} is the standard deviation of the PMT intensity measured in volts, $\mu_{\text{intensity}}$ is the average measured PMT intensity in volts, C is a current to voltage conversion factor, G is the gain of the PMT (unitless), e is the fundamental charge of an electron (1.6×10^{-19} C), f_{3dB} is the 3 dB point in the PMT frequency distribution and is inversely proportional to the measurement time of the PMT. Values for C (0.1 V/μA), G across a range of control voltages, and f_{3dB} (200 kHz) are provided in the PMT spec sheet (0.1 V/μA).[6]

Calculation of Noise. The theoretical estimates of $\sigma_{particle}$ ($\sqrt{\lambda}$) are calculated for an arbitrary range of particle loading values (λ) of microbeads and quantum dots in drops. For microbeads, a range of 10^1 to 10^3 microbeads/drop is used. The number of quantum dots are calculated from the molarity, assuming each particle represents a molecule. Therefore, the particle concentration is calculated as the molarity multiplied by the drop volume (65 pl) and Avogadro's number (≈6.022 × 10^{23} mol^{-1}). A quantum dot concentration range of 1.3 × 10^0 to 1.3 × 10^5 pM is used and corresponds to a particle loading range of 5 × 10^2 to 5 × 10^6 QD/drop. For comparison with the barcode data (Fig. 4c-d, inset), the estimates of $\sigma_{particle}$ (Fig. 4c-d, inset, dashed red line) are converted from particles/drop to voltage using Fig. S7a and Fig. S7c for the microbead and quantum dot cases, respectively. The voltage ranges used for the x-axis are calculated by converting the range of microbead and quantum dot particles per drop to voltages using the respective standard curves in Fig. S7. The same voltage ranges are then used to calculate σ_{shot} from Eq. S1 (Fig. 4c-d, inset, dotted green line).

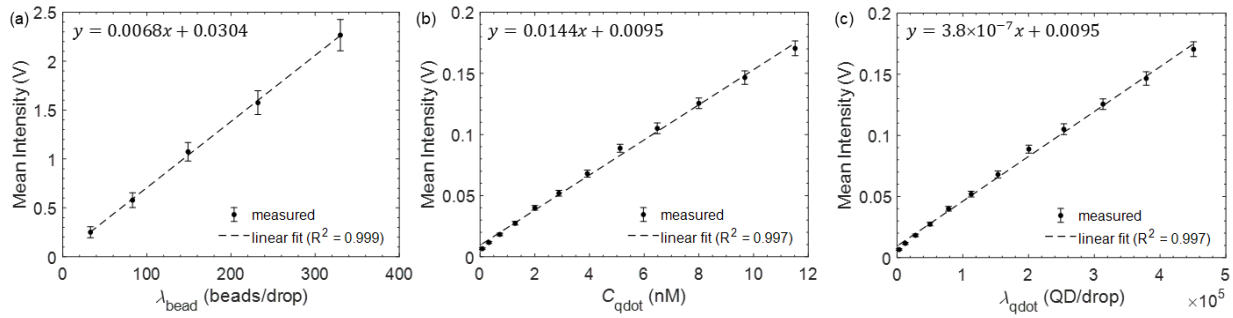

Fig. S7 Standard curves of the mean fluorescence intensity (V) versus (a) the number of microbeads per drop (λ_{bead}), (b) the concentration of quantum dots (C_{qdot}), and (c) number of quantum dots per drop (λ_{qdot}). Error bars represent one standard deviation.

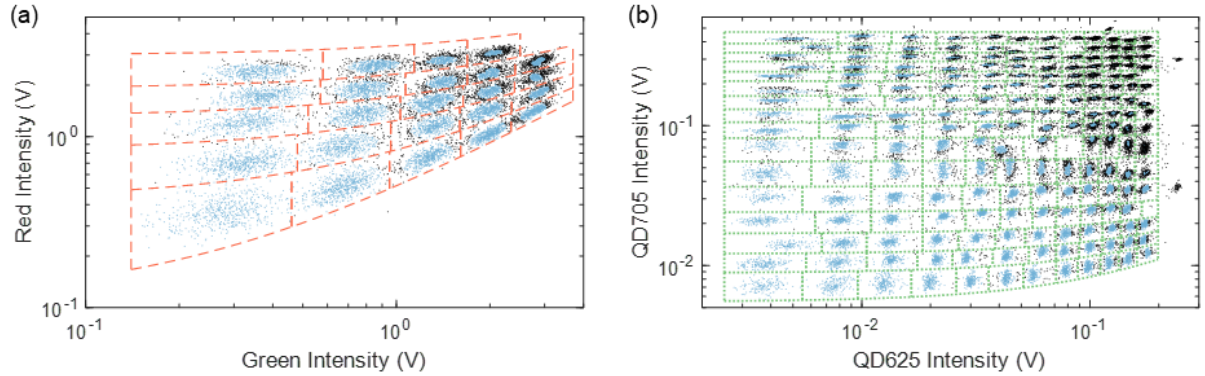

Fig. S8 Manual grouping of barcoded drop library data for (a) microbead and (b) quantum dot barcoded drops indicated by dashed red and dotted green lines, respectively.

6. Supplemental References

1. P. Garstecki, M. J. Fuerstman, H. A. Stone and G. M. Whitesides, *Lab on a Chip*, 2006, **6**, 437-446.

2. L. Mazutis, J. Gilbert, W. L. Ung, D. A. Weitz, A. D. Griffiths and J. A. Heyman, *Nature protocols*, 2013, **8**, 870-891.

3. M. Ester, H.-P. Kriegel, J. Sander and X. Xu, Portland, OR, 1996.

4. W. Schottky, *Annalen der physik*, 1918, **362**, 541-567.

5. R. L. McClain and J. C. Wright, *Journal of Chemical Education*, 2014, **91**, 1455-1457.

6. Hamamatsu, Specification sheet for H10723-20 photomultiplier tube, https://www.hamamatsu.com/resources/pdf/etd/H10723_TPMO1064E.pdf).